

generalization of this invariant. The quantization of the self-linking number is directly related to the geometric, or Berry's, phase (27). For nematic braids, the geometric phase corresponds to the angular shift φ that is acquired upon the parallel transport of a surface normal traveling along one surface of the characteristic three-sided strip. More specifically, the angular shift is equivalent to $\varphi = 2\pi SL$ (Fig. 3A). Eventually, the SL and the number of loops N can be used for a unique classification of all possible loop conformations—that is, all the available knot types on a given $p \times q$ particle array. Figure 3B shows the classification of the topological objects on a three-by-four particle array, determined by testing all the possible combinations of unit tangles. Using SL and N as the characteristic invariants, the knots and links arrange hierarchically and regularly alternate between the knotted/unknotted and linked/unlinked structures (25), which is promising for predicting the complexity of the knots and links that can be realized on a specific $p \times q$ particle array.

Having experimental control over the knotting and having theoretical tools for finding all possible conformations of nematic braids, we were able to perform a made-to-order assembly of knots and links, illustrated in Fig. 3C. First, we selected Borromean rings (23) as an example of a complex interwoven structure, which we attempted to weave. Next, we specified the size of the particle array to be four by four, the smallest array required for the chosen link. By using a computer algorithm that is based on calculating the polynomial invariants from knot theory (fig. S2) (23, 28, 29), the tangle configuration that corresponds to the chosen link was identified. The site-specific pattern of tangles shown in Fig. 3C (fourth frame) was needed. Lastly, we experimentally assembled the Borromean rings using laser tweezers. To show the reach of our assembly method, we present all of the prime knots and links that can be made to order on a four-by-four particle array in Fig. 3D. Almost 40 dif-

ferent knot and link types are discerned among $3^{(p-1)(q-1)} = 3^9$ tangle combinations with minimum crossing numbers up to 10. Out of all the loop conformations, 35% are prime knots or links, 29% are unknots, 18% are unlinks, and 18% are more complex composite links (table S1). Such a large diversity of topological objects suggests that it is possible to design any knot or link on a sufficiently large colloidal array.

We have shown that chiral nematic colloids are stabilized by defect knots and links of fascinating complexity, which can be fully controlled and rewired by light. This unusual colloidal soft-matter system provides a robust made-to-order assembly of an arbitrary knot or link on a microscopic scale and is a new route to the fabrication of soft matter with special topological features. We believe that the strategy presented here offers guidance to further progress in our understanding of the knotting of topologically nontrivial entities, such as DNA (5), skyrmion lattices in chiral magnets (30) and confined blue phases (31), and entangled vortices in superconductors (32).

References and Notes

- C. C. Adams, *The Knot Book* (American Mathematical Society, Providence, 2004).
- L. H. Kauffman, *Knots and Physics* (World Scientific Publishing, Singapore, ed. 3, 2000).
- J. P. Sauvage, C. Dietrich-Buchecker, Eds., *Molecular Catenanes, Rotaxanes and Knots: A Journey Through the World of Molecular Topology* (Wiley, Weinheim, 1999).
- K. S. Chichak *et al.*, *Science* **304**, 1308 (2004).
- D. Han, S. Pal, Y. Liu, H. Yan, *Nat. Nanotechnol.* **5**, 712 (2010).
- P. G. de Gennes, *Scaling Concepts in Polymer Physics* (Cornell Univ. Press, New York, 1979).
- L. Faddeev, A. J. Niemi, *Nature* **387**, 58 (1997).
- W. T. M. Irvine, D. Bouwmeester, *Nat. Phys.* **4**, 716 (2008).
- M. R. Dennis, R. P. King, B. Jack, K. O'Holleran, M. J. Padgett, *Nat. Phys.* **6**, 118 (2010).
- A. D. Bates, A. Maxwell, *DNA Topology* (Oxford Univ. Press, Oxford, ed. 2, 2005).
- D. Meluzzi, D. E. Smith, G. Arya, *Annu. Rev. Biophys.* **39**, 349 (2010).
- Y. Bouligand, *J. Phys. (Paris)* **35**, 215 (1974).
- P. G. de Gennes, J. Prost, *The Physics of Liquid Crystals* (Oxford Science Publications, Oxford, 1993).
- N. D. Mermin, *Rev. Mod. Phys.* **51**, 591 (1979).
- P. Poulin, H. Stark, T. C. Lubensky, D. A. Weitz, *Science* **275**, 1770 (1997).
- H. Stark, *Phys. Rep.* **351**, 387 (2001).
- D. G. Grier, *Nature* **424**, 810 (2003).
- M. Yada, J. Yamamoto, H. Yokoyama, *Phys. Rev. Lett.* **92**, 185501 (2004).
- I. Mušević *et al.*, *Phys. Rev. Lett.* **93**, 187801 (2004).
- I. Mušević, M. Škarabot, U. Tkalec, M. Ravnik, S. Žumer, *Science* **313**, 954 (2006).
- T. Araki, H. Tanaka, *Phys. Rev. Lett.* **97**, 127801 (2006).
- M. Ravnik *et al.*, *Phys. Rev. Lett.* **99**, 247801 (2007).
- Materials and methods are available as supporting material on Science Online.
- V. V. Prasolov, A. B. Sossinsky, *Knots, Links, Braids and 3-Manifolds* (American Mathematical Society, Providence, RI, 1997).
- S. Čopar, S. Žumer, *Phys. Rev. Lett.* **106**, 177801 (2011).
- J. H. White, *Am. J. Math.* **91**, 693 (1969).
- F. Wilczek, A. Shapere, Eds., *Geometric Phases in Physics* (World Scientific Publishing, Singapore, 1988).
- D. M. Raymer, D. E. Smith, *Proc. Natl. Acad. Sci. U.S.A.* **104**, 16432 (2007).
- J. C. Cha, C. Livingston, *KnotInfo: Table of Knot Invariants*; <http://www.indiana.edu/~knotinfo> (2011).
- S. Mühlbauer *et al.*, *Science* **323**, 915 (2009).
- J. Fukuda, S. Žumer, *Nat. Commun.* **2**, 246 (2011).
- D. R. Nelson, *Nature* **430**, 839 (2004).
- R. G. Sharein, thesis, University of British Columbia (1998).

Acknowledgments: U.T. thanks S. Herminghaus, S. Kralj, and S. Vrtnik for discussions and kindly acknowledges support of the Max Planck Society. M.R. acknowledges support of the European Commission (EC) under the Marie Curie Program Active Liquid Crystal Colloids (ACTOIDS); content reflects only the authors' views and not the views of the EC. The research was funded by Slovenian Research Agency under the contracts P1-0099, PR-00182, and J1-9728 and in part by the NAMASTE Center of Excellence.

Supporting Online Material

www.sciencemag.org/cgi/content/full/333/6038/62/DC1
Materials and Methods
Figs. S1 and S2
Table S1
References (34–43)
Movies S1 to S3

16 March 2011; accepted 12 May 2011
10.1126/science.1205705

Rotary Photon Drag Enhanced by a Slow-Light Medium

Sonja Franke-Arnold,^{1*} Graham Gibson,¹ Robert W. Boyd,^{2,3} Miles J. Padgett¹

Transmission through a spinning window slightly rotates the polarization of the light, typically by a microradian. It has been predicted that the same mechanism should also rotate an image. Because this rotary photon drag has a contribution that is inversely proportional to the group velocity, the image rotation is expected to increase in a slow-light medium. Using a ruby window under conditions for coherent population oscillations, we induced an effective group index of about 1 million. The resulting rotation angle was large enough to be observed by the eye. This result shows that rotary photon drag applies to images as well as polarization. The possibility of switching between different rotation states may offer new opportunities for controlled image coding.

The speed of light is independent of the choice of reference frame only in a vacuum. Once light enters a moving medium, it can be dragged in either the transverse or lon-

gitudinal direction. This phenomenon was first considered by Fresnel in 1818 (1) and then, for the longitudinal case, verified by Fizeau (1859), who used water flowing along the light paths

within an interferometer as a means of introducing a phase shift (2). Over 100 years later, the transverse displacement of a beam transmitted near the edge of a spinning glass disk was observed (3). A similar setup allowed the study of a closely related effect for light traveling along the rotation axis of a spinning medium, which results in the rotation of the optical polarization state (4, 5), the mechanical Faraday effect (6).

The rotation of a linear polarization state originates from a phase difference between the right- and left-handed circular polarization states,

¹School of Physics and Astronomy (SUPA), University of Glasgow, Glasgow G12 8QQ, Scotland. ²Department of Physics, University of Ottawa, Ottawa, ON K1N 6N5, Canada. ³The Institute of Optics and Department of Physics and Astronomy, University of Rochester, Rochester, NY 14627, USA.

*To whom correspondence should be addressed. E-mail: sonja.franke-arnold@glasgow.ac.uk

which are the spin angular momentum states of light. However, light can also carry orbital angular momentum (OAM) arising from helical phase fronts and the associated azimuthal component of the Poynting vector (7). For a transverse phase profile given by $\exp(i\ell\phi)$, where ϕ describes the azimuthal angle, the OAM corresponds to $\ell\hbar$ per photon.

Whereas a phase shift between the spin angular momentum states leads to a rotation of the linear polarization state, a phase shift between the components with positive and negative OAM is manifested as a rotation of the transmitted intensity profile (8). A mechanical rotation of a medium is predicted to induce a rotational photon drag (9, 10), rotating the transmitted polarization state and the transmitted image through the same angle

$$\Delta\phi = \left(n_g - \frac{1}{n_\phi} \right) \frac{\Omega L}{c} \quad (1)$$

Here, n_g and n_ϕ are the group and phase refractive index, respectively; Ω is the angular frequency at which the medium rotates, L is the length of the medium, and c is the speed of light in a vacuum.

For a typical dielectric material with a window thickness of a few tens of millimeters and a rotation rate of ~ 1000 rpm, the resulting angle is on the order of a microradian. Although the rotation of polarization has been observed (4), the corresponding image rotation has not.

The small rotation angle makes a measurement very difficult, and as an alternative, we previously examined a rapidly spinning image incident upon a stationary window, where a megahertz rotation rate gave a delay in the spinning of the image by ~ 1 rad (11). A spinning image is just a superposition of beams at different frequencies that can be treated separately in a linear medium. In that experiment, however, the effect was complicated by the Galilean transformation of the frame that modified the incident angle of the light upon the interfaces and, through Snell's law, the angular displacement of the transmitted light. Because of this transformation, the lag in rotation arose simply from the delay in arrival time of the light due to the thickness of the optical medium, i.e., $(n_g - 1)\Omega L/c$ (12).

Rather than measuring the rotational lag between two images, our present experiment directly observes the rotation of the image, which becomes feasible when the angle of the rotation is enhanced by use of a slow-light medium. We used a ruby rod as the spinning medium and a stationary elliptical laser beam at 532 nm to act as the image. Ruby is an unusual material in that, by illuminating it with green light, one can probe an absorption that acts as a near perfect two-level system with a long (≈ 20 ms) upper-state lifetime. If the incident beam is subject to a slight temporal intensity modulation, the resulting modulation in the lower-state population leads to a modulation of the absorption that is, due to the long upper-state lifetime, slightly out of phase with the mod-

ulation of the incident intensity. This phase lag in the absorption distorts the intensity modulation of the transmitted light, resulting in an optical delay that is interpreted as a large group index.

The effective group index depends upon many factors, including the intensity and modulation amplitude of the light compared to the saturation intensity, and the modulation frequency compared to the inverse of the upper-state lifetime. Previously it had been shown that group indices of $\approx 10^6$ may be obtained from coherent population modulations (13–15).

When viewed in a rotating frame, the right- and left-handed helical states are subject to a rotational frequency shift (16, 17), which, because of the dispersion of the ruby, means that their phase indices differ. A phase shift therefore accumulates between the states upon propagation through the medium, leading to a rotation of the resulting image.

An image rotation is defined only if the incident light is not rotationally symmetric; for simplicity we have chosen an elliptical beam profile. This beam profile also provides the intensity modulation that causes a large group index in ruby. Even for a beam with constant intensity, the off-axis atoms in the spinning ruby rod experi-

ence an intensity modulation. The resulting delay and associated group index in general is a function of radius, intensity, and modulation rate and must be evaluated numerically (see supporting online material). For rotation speeds that are slow compared to the inverse of the upper-state lifetime, the group index is large. At higher speeds, the effect saturates and the group index decreases. Consequently, for rotation rates below that corresponding to the inverse of the upper-state lifetime, we anticipate a large effective group index, leading to substantial rotational drag of the transmitted beam profile.

In a preliminary experiment, we used a highly elliptical 2-W laser beam at 532 nm, focused through a 100-mm-long ruby rod. By focusing the beam into the ruby, it is possible to reach a high intensity, albeit with a complicated beam profile that changes upon propagation and makes the configuration hard to model. After transmission through the rod, the beam cross section is a single line that is readily observed on a viewing screen. Spinning the ruby rod at ≈ 30 Hz drags the orientation of the line by $\sim 5^\circ$. Figure 1 shows two images of the line for clockwise and anti-clockwise rotation, respectively (also see movie

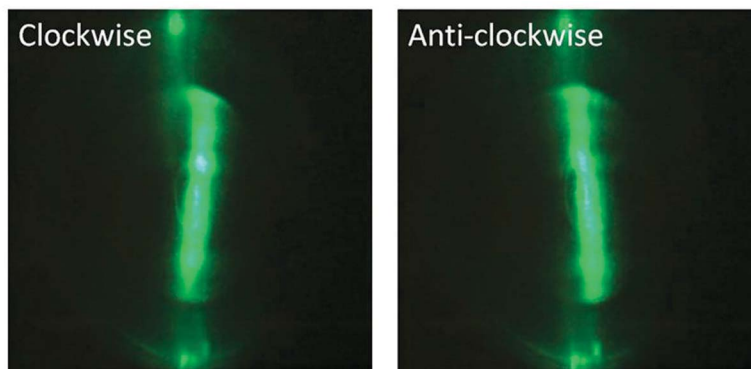


Fig. 1. An intense line of laser light is focused through a 100-mm-long ruby rod. The images show the transmitted intensity as recorded on a screen positioned ~ 500 mm behind the rod spinning at ± 30 Hz. The difference in line orientation between the two directions is $\sim 10^\circ$. The fixed light at the top and bottom of the images is transmitted around the sides of the ruby and hence not subject to any rotation.

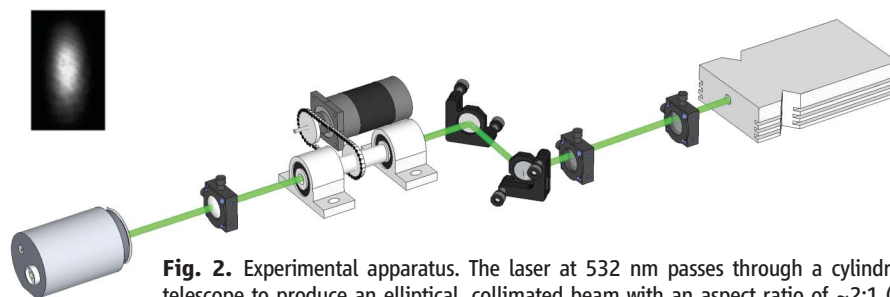


Fig. 2. Experimental apparatus. The laser at 532 nm passes through a cylindrical telescope to produce an elliptical, collimated beam with an aspect ratio of $\sim 2:1$ (see inset). The light is transmitted axially through a rotating ruby rod and monitored on a CCD camera. The ruby rod is mounted within a hollow cylinder, itself mounted within a standard engineering high-speed bearing. The rotation of the ruby rod is controlled by a servo-controlled, programmable stepper motor at up to ± 30 Hz.

S1). We attribute this rotation of the beam to the rotary image drag, enhanced by the high group index in the ruby. Within the limits of experimental observation, the resulting transmitted intensity pattern appears as a rotated line, as one would expect from a simple interpretation of rotary image drag in Eq. 1.

To quantitatively investigate the effect of rotary image drag in a self-pumped slow-light medium, we instead propagated a collimated elliptical beam through a 6-mm length of ruby rod spinning at up to 30 Hz, observing rotations of the intensity profile of some tenths of a degree.

The experimental setup is shown in Fig. 2. The collimated elliptical laser beam with major and minor axes of 2 mm and 0.9 mm, respectively (see inset of Fig. 2), was incident on the ruby rod, colinear with its rotation axis. The exit face of the rod was imaged with unity magnification to a low-noise charge-coupled device (CCD) detector array. The orientation of the elliptical intensity cross section was then analyzed from the CCD image with respect to its center in terms of its second-order moments to determine the angle between the major axis of the elliptical profile and the camera horizontal. For each rotation speed, the sense of rotation was switched several times over a period of a few seconds, and the

average difference in orientation of the major axis was recorded (Fig. 3 shows a typical recording). The process was repeated for each rotation speed and for two different levels of laser power (Fig. 4). For a constant group index of the medium, the rotation of the transmitted beam would simply be proportional to the rotational speed. However, in our case, the group index and hence the phase delay is itself a function of that speed (fig. S2), resulting in a leveling-off of the orientation angle for higher rotation speeds.

The vertical scaling of the data depends upon the saturation intensity and precise beam size, and therefore the total power of the beam was set as a free parameter within a 30% range of its measured value. The level of agreement between observations and predicted forms of the data is good, both with respect to the lower-speed linear growth of the image rotation and the higher-speed saturation that occurs when the rotation period is less than the upper-state lifetime of the ruby.

Our results show that the phenomenon of rotary photon drag applies not just to linear motion and image displacement, but also to rotational motion and image rotation. The Faraday effect arising from the mechanically induced difference in phase velocity for right- and left-handed cir-

cularly polarized light has an equivalent effect for orbital angular momentum. For orbital angular momentum, the difference in phase velocity results in a phase shift between right- and left-handed helical phase fronts, giving an image rotation. The observed rotation is compatible with the two rotation angles for polarization and image being the same.

References and Notes

1. A. Fresnel, *Ann. Chim. Physique* **9**, 57 (1818).
2. M. H. Fizeau, *Ann. Chim. Phys.* **57**, 385 (1859); *Philos. Mag.* **19**, 245 (1860).
3. R. V. Jones, *Proc. R. Soc. London A Math. Phys. Sci.* **328**, 337 (1972).
4. R. V. Jones, *Proc. R. Soc. London A Math. Phys. Sci.* **349**, 423 (1976).
5. M. A. Player, *Proc. R. Soc. London A Math. Phys. Sci.* **349**, 441 (1976).
6. G. Nienhuis, J. P. Woerdman, I. Kuscer, *Phys. Rev. A* **46**, 7079 (1992).
7. L. Allen, M. W. Beijersbergen, R. J. C. Spreeuw, J. P. Woerdman, *Phys. Rev. A* **45**, 8185 (1992).
8. L. Allen, M. Padgett, *J. Mod. Opt.* **54**, 487 (2007).
9. M. Padgett *et al.*, *Opt. Lett.* **31**, 2205 (2006).
10. J. B. Götte, S. M. Barnett, M. Padgett, *Proc. R. Soc. London A* **463**, 2185 (2007).
11. J. Leach *et al.*, *Phys. Rev. Lett.* **100**, 153902 (2008).
12. The functional dependence with regard to the phase index differs between the propagation of a spinning image through a stationary rod and a stationary image through a spinning medium (Eq. 1). However, this difference becomes experimentally negligible in a slow-light medium where the large group index dominates.
13. M. S. Bigelow, N. N. Lepeshkin, R. W. Boyd, *Phys. Rev. Lett.* **90**, 113903 (2003).
14. M. S. Bigelow, N. N. Lepeshkin, R. W. Boyd, *Science* **301**, 200 (2003).
15. A. Schweinsberg, N. N. Lepeshkin, M. S. Bigelow, R. W. Boyd, S. Jarabo, *Europhys. Lett.* **73**, 218 (2006).
16. B. A. Garetz, *J. Opt. Soc. Am.* **71**, 609 (1981).
17. J. Courtial, D. A. Robertson, K. Dholakia, L. Allen, M. J. Padgett, *Phys. Rev. Lett.* **81**, 4828 (1998).
18. G. Piredda, R. W. Boyd, *J. Eur. Opt. Soc.* **2**, 07004 (2007).

Acknowledgments: This work is supported by the UK Engineering and Physical Sciences Research Council. M.J.P. thanks the Royal Society and the Wolfson Foundation. We acknowledge the financial support of the Future and Emerging Technologies (FET) program for Research of the European Commission, under the FET Open grant agreement PHORBITECH number FP7-ICT-255914. R.W.B. acknowledges support from the Defense Advanced Research Projects Agency (DARPA)—DSO Slow Light Program and from the Defense Threat Reduction Agency—Joint Science and Technology Office for Chemical and Biological Defense (grant HDTRA1-10-1-0025). The enhancement of image rotation in a slow-light medium was proposed by S.F.-A. and R.W.B., based on the spinning window for image drag previously investigated by M.J.P. The theoretical analysis was devised by S.F.A. and R.B. and performed by S.F.A. The experiment was designed by G.G. and M.J.P. and performed by G.G. All authors contributed to the writing of the manuscript.

Supporting Online Material

www.sciencemag.org/cgi/content/full/333/6038/65/DC1
Materials and Methods
Figs. S1 to S3
References
Movie S1

8 February 2011; accepted 27 April 2011
10.1126/science.1203984

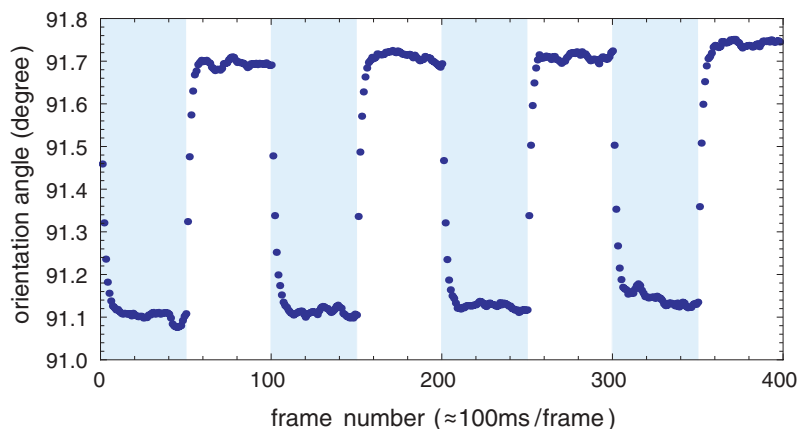


Fig. 3. Typical data of the orientation of the major axis of the elliptical beam profile for rotation speeds switched between ± 14 Hz.

Fig. 4. Rotation angle of the elliptical laser beam upon passage through a 6-mm-long ruby rod for a beam power of 1 W (blue, green) and 2 W (red, orange, purple). The solid lines are theoretical predictions of the model described in the supporting online material. The rotation angle is taken to be half the difference of the measured values for the ruby spinning in the forward and backward directions.

